Contemporary Mathematics
https://ojs.wiserpub.com/index.php/CM/

Research Article

Application of Horizontal Visibility Graph in Time Series Analysis of Emergency Department Diseases and Mining of Infectious Disease Characteristics

Linyuan Zhang[1], Yuqi Liu[2], Man Zhou[2], Kezhao Xiong[2,3], Li Zhang[4], Chao Wu[1], Jian Liu[5,6], Hongjuan Lang[1]*

[1] School of Nursing, Air Force Medical University, Xi'an, 710032, P. R. China
[2] College of Sciences, Xi'an University of Science and Technology, Xi'an, 710054, P. R. China
[3] Department of Physics, Fudan University, Shanghai, 200433, P. R. China
[4] Department of Emergency Medicine, The First Affiliated Hospital, Air Force Medical University, Xi'an, 710032, P. R. China
[5] Teaching and Research Support Center, Air Force Medical University, Xi'an, 710032, P. R. China
[6] The Third Affiliated Hospital, Air Force Medical University, Xi'an, 710032, P. R. China
E-mail: langhj@fmmu.edu.cn

Received: 19 May 2025; **Revised:** 28 September 2025; **Accepted:** 13 October 2025

Abstract: The conversion of time series into visualized networks is one of the most important tools for comprehending data patterns and trends. This study pioneers the application of a Horizontal Visibility Graph (HVG) algorithm to transform hospital emergency department time series into complex networks. By analyzing the topological characteristics of networks across different disease categories, we found that all networks exhibit significant small-world properties. Moreover, we observed that the average degree of the networks is notably higher for respiratory diseases. Most importantly, networks of respiratory diseases demonstrate larger maximum eigenvalues of the Laplace matrix, which are closely associated with their stronger infectious potential. These findings reveal the structural signatures of disease spread and provide a critical analytical tool for building network-based early warning systems for specific infectious diseases and triage optimization.

***Keywords*:** complex networks, topological characteristic, Laplace matrix

MSC: 62H30, 05C82, 68U05

1. Introduction

Over the past decades, the rise of complex network theory has spurred extensive interdisciplinary research, attracting scholars from diverse fields to integrate network-based approaches into their respective domains [1–5]. In medicine, complex networks have been employed to model disease comorbidity and drug interaction patterns [6, 7]. In physics, researchers examine how network topology influences physical processes and emergent behaviors [8–10]. Sociologists leverage social networks to uncover structural dynamics in human relationships and organizations [11], while biologists use network models to map interactions within protein-protein or genetic regulatory systems [12]. Economists, likewise,

DOI: https://doi.org/10.37256/cm.7120267259

apply network analysis to decipher the complex interdependencies driving economic fluctuations and systemic risks [13]. Notably, in the domain of engineering safety and risk assessment, the construction of risk propagation networks for tailings dam failures has allowed accurate identification of critical hazard sources underlying system failures [14]. Thus, the application of complex networks continues to expand across an growing array of disciplines, reflecting its vitality and broad relevance.

As pointed out above, complex network theory has a wide range of applications in the field of medicine [15]. Medical practitioners have already started to analyze treatment situations or outcomes in conjunction with complex networks in order to improve and optimize later treatments or modalities [16–18]. For example, the Symptom Multilayer Network [19, 20] integrates different levels of symptom relationships into a unified network framework. This allows researchers to systematically understand how disease symptoms interact and affect a patient's overall health and quality of life. The Symptom Simultaneous Network [21] is a model used to study the synchronous occurrence and interconnection of disease symptoms. It aims to reveal the synchronicity between these symptoms, providing a deeper understanding of disease manifestation and progression. Disease transmission model [22, 23], through complex network theory can establish a disease transmission model, by analyzing the interpersonal network or disease transmission network, the speed, path and scale of disease transmission can be predicted, which can help to formulate corresponding preventive measures and responsive strategies. To summarize, complex network theory provides a fresh perspective and analytical tool for medical research, which helps to deeply understand the mechanism of disease occurrence and progression, and promotes the early diagnosis, prevention and treatment of diseases.

In addition, the clinical data in medicine can be transformed into a complex network through the method of time series [24, 25], which can be used to analyze the characteristics of the disease by studying the topology of the network, thereby facilitating more effective treatments or interventions. For example, constructing the clinical data between different patients into a complex network can reveal the interrelations and propagation patterns between diseases, which helps to comprehend the epidemiological characteristics and disease propagation mechanisms, and provides a foundational reference for disease control and prevention [26]. Models based on complex networks can forecast disease progression or treatment efficacy for individual patients, preemptively identifying potential complications or deteriorations, thus allowing for appropriate interventions [27]. constructing the numbers of daily patient visits into complex networks can predict the number of daily patient visits, which will help hospital administrators in optimizing and distributing medical personnel during decision-making processes [28]. In view of this, this paper adopts a similar time series visualisation network method to convert the hospital emergency data into a complex network [29, 30]. Through a detailed analysis of the network's structural characteristics and an in-depth examination of the eigenvalue spectrum of the Laplacian matrix of the network corresponding to various disease categories, we observe that the maximum eigenvalue of the Laplacian matrix for respiratory diseases is generally higher than other categories of diseases.

Specifically, we count the emergency room data (data from the Department of Emergency Medicine, The First Affiliated Hospital, Air Force Medical University) for a total of 16 diseases in four categories from January 2017 to June 2023 over 78 months. We convert this time-series data into a visualization network, and investigate condition characteristics by examining network topology. First, we compute fundamental structural statistical parameters of the network, including the average degree $< k >$, the average shortest path $< d >$, the number of community structures S, and the clustering coefficient C. We find that the clustering coefficients are high for all diseases. Notably, respiratory diseases exhibit a higher average shortest path compared to other disease categories, suggesting a stronger small-world effect in respiratory diseases. In addition, we observe that respiratory diseases display lower average degrees to other disease categories, indicating the existence of obvious differences between respiratory diseases and other diseases categories. Furthermore, we find that the maximum eigenvalue of the network is correlated with the infection of the disease by calculating the eigenvalue distribution of the network. Specifically, the maximum eigenvalues of respiratory diseases are generally higher than those of other categories of diseases. Therefore, we utilize the maximum eigenvalue $\omega_{\max}$ as an indicator of disease infection, facilitating targeted preventive measures.

2. Methods

2.1 *Data availability statement*

Data is provided within the manuscript. We obtained data from the Department of Emergency Medicine, The First Affiliated Hospital, Air Force Medical University, covering the period from January 2017 to June 2023 (78 months). The dataset includes time series for 16 diseases across four categories, which were used to construct network structures and study the differences between respiratory and other diseases at the network science level. The data samples were provided by L. Z. from the same department.

2.2 *Statistical analysis*

The Horizontal Visibility Graph (HVG) is a method that converts a time series into a graph while preserving the inherent characteristics of the original series [31]. As a geometric simplification of the initially proposed Visibility Graph (VG) [32], the HVG represents each point in the time series as a node in the graph. Connections between nodes are formed based on the following criterion: given a time series $\{x_i,\ i = 1,\ \cdots,\ N\}$, two nodes i and j are connected if a horizontal line can be drawn between x_i and x_j without intersecting any intermediate data points. In other words, $x_i,\ x_j > x_n$ for all n between i and j. This construction ensures temporal adjacency is inherently incorporated into the network structure.

In the HVG, each node is at least connected to its immediate neighbors, thereby naturally incorporating temporal causality. One notable property of the HVG is its invariance under rescaling and translation of both the horizontal and vertical axes [31, 33].

The emergency department time series data were converted into complex networks using the HVG algorithm. The time series data were aggregated into regular 10-day intervals, specifically the first 10 days, the middle 10 days, and the last 10 days of each month (including the months with less than 30 days and more than 30 days), representing case frequencies for each disease category. Subsequently, we sorted them by month to generate a time series graph, where the horizontal coordinate x represents a statistical data formed every 10 days, and the vertical coordinate y represents the frequency of occurrences, as illustrated in Figure 1a. Let $(x_a,\ y_a)$ and $(x_b,\ y_b)$, be two distinct points of a time series. Take any other point $(x_c,\ y_c)$ between them. The points $(x_a,\ y_a)$ and $(x_b,\ y_b)$ are considered visually related if the following rule is satisfied [34]

$$x_c < x_a + (x_b - x_a)\frac{y_c - y_a}{y_b - y_a}. \tag{1}$$

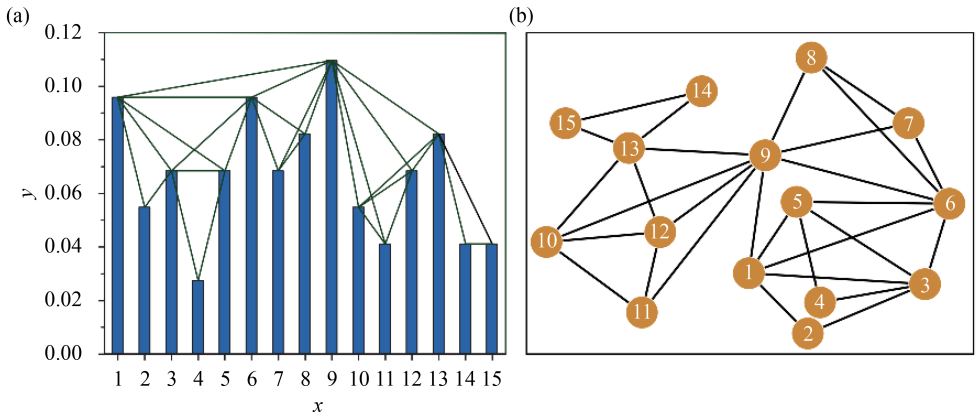

Figure 1. Scheme for visibility graph approach. (a) A 15-elements time series is mapped into a graph where each node represents a bar, and each edge represents the connection between two bars. (b) Schematic representation of the time series of (a) transformed into a complex network

In Figure 1, the i-th bar represents the i-th statistical data point. Figure 1a illustrates an example time series composed of 15 data points, depicted as vertical bars. Line segments connect pairs of data points that are mutually 'visible'-that is, the line between them does not intersect any intermediate data points. This visibility criterion, formalized in Eq. (1), is visually demonstrated in Figure 1a. Figure 1b presents the resulting network structure after applying the HVG algorithm to the time series shown in Figure 1a. Each data point is mapped to a node in the network, and every visibility relation is represented as an edge connecting the corresponding nodes. This network effectively captures the mutual visibility relationships among the time series data. Overall, the visibility graph method transforms a time series into a complex network, where each observation becomes a vertex, as depicted in Figure 1b.

We counted the time series for four different disease categories and converted them into a network structure. Each disease category comprised four distinct diseases spanning from January 2017 to June 2023. The total number of nodes $N = 234$ in the network according to the rule of counting 3 times per month. In addition, in order to analyse the topology of the network more efficiently, we calculated four commonly used structural statistical parameters: (1) The average degree $< k >$ [35], which represents the closeness of connected edges in the network and is calculated as $< k >= \frac{1}{N}\sum_i k_i$, where k_i denotes the degree of i-th node. (2) The cluster coefficient C [35], which represents the proportion of a node's neighbours that are also neighbours with each other, and is calculated as $C =< C_i >= \frac{1}{N}\sum_i C_i$, where $C_i = \frac{2l_i}{k_i(k_i-1)}$, l_i denotes the number of connected edges between i-th node's neighbours. (3) The average shortest path in the network $< d >$ [35], which denotes the network's average distance between any two nodes, and is calculated as $< d >= \frac{1}{N}\sum_i < d_i >$, where $< d_i >$ denotes the average shortest path from i-th node to all other nodes in the network. (4) The number of community structures in the network S [35, 36], which denotes the number of different groups within the network.

3. Results

3.1 *Analysis from structural statistics*

We begin our analysis with the first category of diseases, which comprises respiratory illnesses. As representative cases, we focus on two specific conditions: respiratory tract infections and pulmonary infections. Figure 2 presents both the original time series data and the complex network structures derived from them for these two diseases. Through quantitative analysis, we observe that the clustering coefficients C for both networks reach considerably high values-approximately 0.786 for respiratory tract infections and 0.788 for pulmonary infections-indicating strong local interconnectivity. The slight difference between these values reflects remarkable consistency in clustering behavior, a characteristic we attribute to the HVG methodology employed in network construction. According to the linking criterion formalized in Eq. (1), a connection is established between two nodes if no intermediate data point obstructs the horizontal line between them. This rule inherently favors connections between temporally adjacent nodes, greatly increasing the probability that neighboring nodes also connect to each other. As a result, triangular substructures are frequently formed, leading to high clustering coefficients across all networks generated by this method, with only minimal variation between different diseases. In addition, both networks exhibit notably short average path lengths $< d >$, measuring 2.64 for respiratory tract infections and 2.69 for pulmonary infections, respectively. Such values indicate high global efficiency in the network, where any two nodes can be connected through very few steps. The co-occurrence of high clustering coefficients and short average path lengths-a hallmark of small-world topology-strongly suggests that these disease networks exhibit significant small-world characteristics [37], which may reflect the contagious and rapidly spreading nature of respiratory diseases.

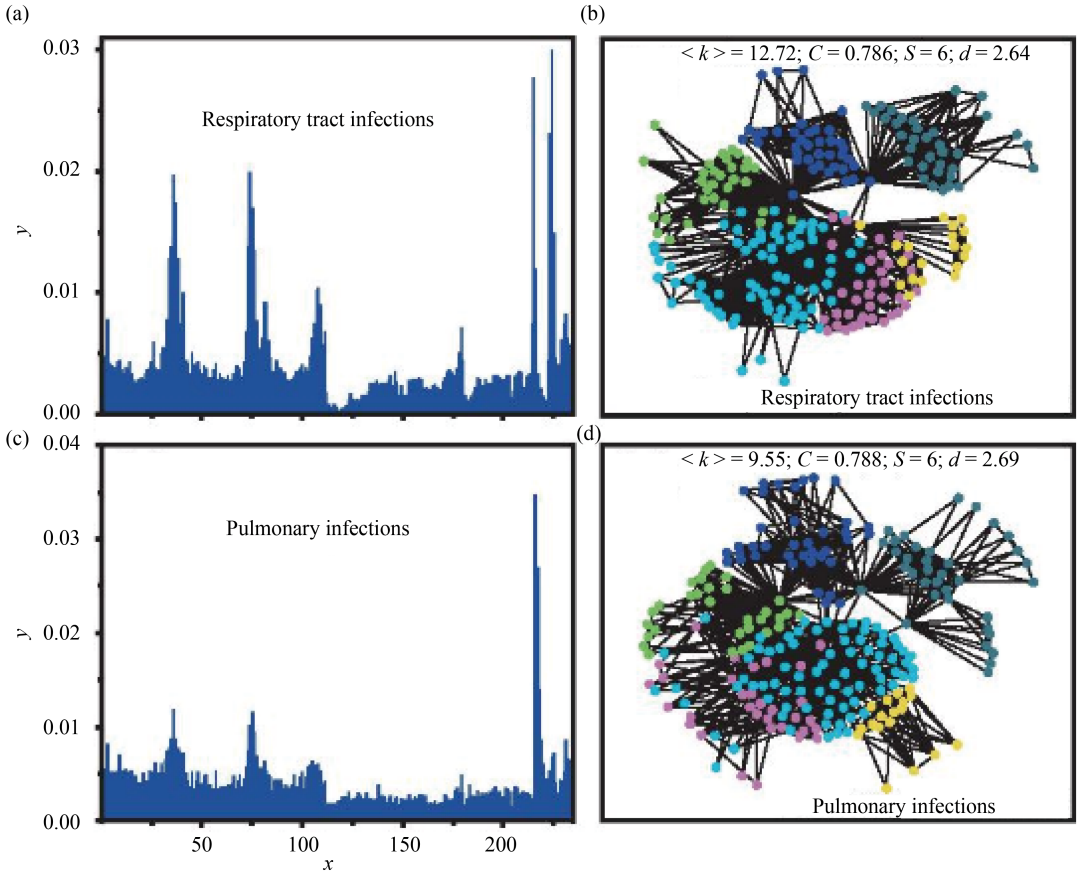

Figure 2. Time series and network structure of two respiratory diseases. (a) and (c) are the time series of respiratory tract infections and pulmonary infections, respectively. (b) and (d) are their corresponding network structures, respectively. Different colors represent different communities

Then we extended our analysis to the category of digestive diseases, selecting acute gastroenteritis and gallstones as representative cases. The time series and corresponding network architectures for these two diseases are illustrated in Figure 3. Quantitative evaluation revealed that both networks exhibit high clustering coefficients $C = 0.70$ for Acute Gastroenteritis and 6.19 for gallstones-accompanied by low average shortest path lengths $< d >$, recorded at 3.67 and 4.12, respectively. These topological traits are indicative of a pronounced small-world effect [37], suggesting efficient local and global connectivity within the networks.

A comparative assessment with the respiratory disease networks presented in Figure 2 reveals notable distinctions: while the respiratory networks display a higher average degree $< k >= 12.72$ for respiratory tract infections and 9.55 for pulmonary infections, compared to values around 7.00 and 6.19 for the digestive diseases-they also maintain shorter average path lengths. This combination of higher connectivity and shorter inter-node distances implies that respiratory disease networks are more densely interconnected, facilitating faster and more efficient propagation of information-or infection. The structural differences underscore a tighter and more cohesive network organization in respiratory diseases, which may mirror their heightened contagious nature and rapid transmission dynamics.

Next, we analyzed two representative circulatory diseases-Hypertension and Venous thrombosis-whose time series and corresponding network topologies are depicted in Figure 4. Both networks demonstrate consistently high clustering coefficients, with values of $C = 0.758$ for Hypertension and $C = 0.761$ for venous thrombosis, as well as short average path lengths, measuring $< d >= 3.43$ and $< d >= 3.45$, respectively. These structural characteristics confirm the presence of a marked small-world effect within circulatory disease networks. Furthermore, community detection revealed a greater number of modular structures S in circulatory disease networks compared to both respiratory and digestive categories. Notably, the average degree $< k >$ of these circulatory networks-approximately 7.15 for Hypertension and 6.32 for venous

thrombosis-is significantly lower than that observed in respiratory disease networks. This suggests a sparser yet efficiently organized connectivity pattern.

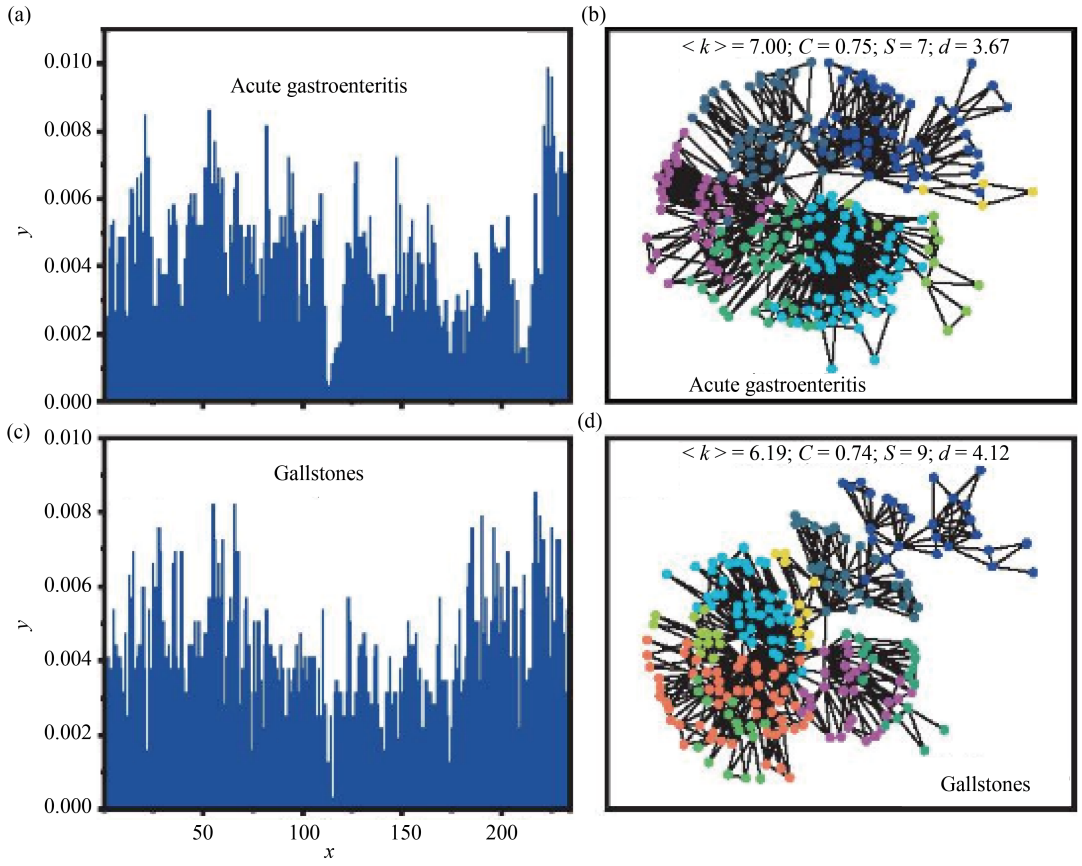

Figure 3. Time series and network structure of two digestive diseases. (a) and (c) are the time series of acute gastroenteritis and gallstones, respectively. (b) and (d) are their corresponding network structures, respectively. Different colors represent different communities

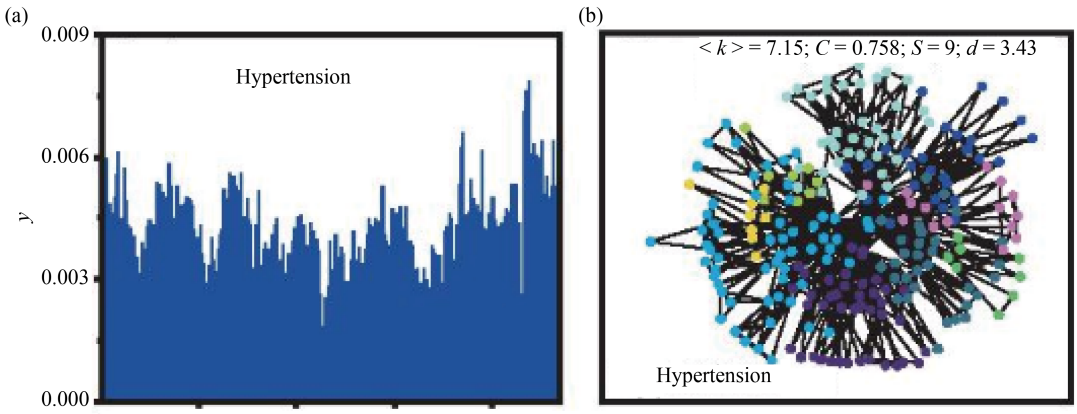

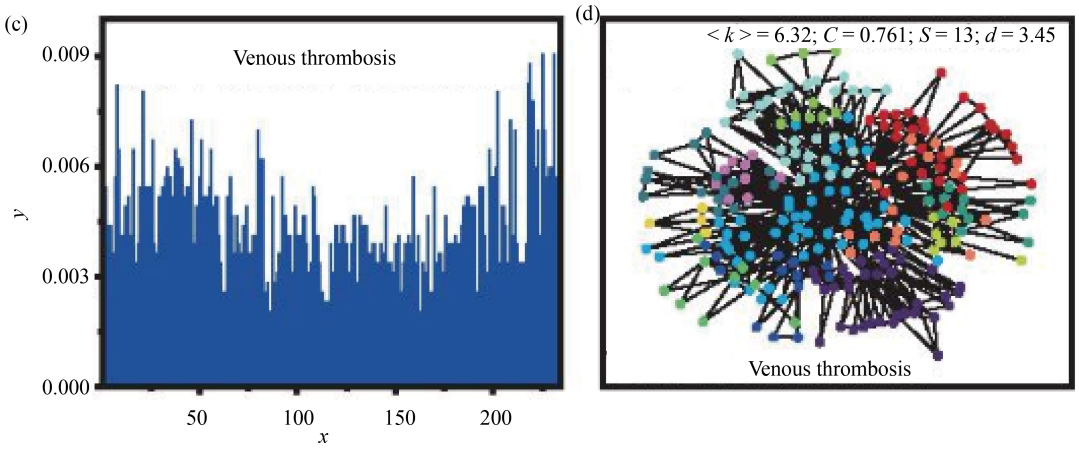

Figure 4. Time series and network structure of two circulatory diseases. (a) and (c) are the time series of Hypertension and venous thrombosis, respectively. (b) and (d) are their corresponding network structures, respectively. Different colors represent different communities

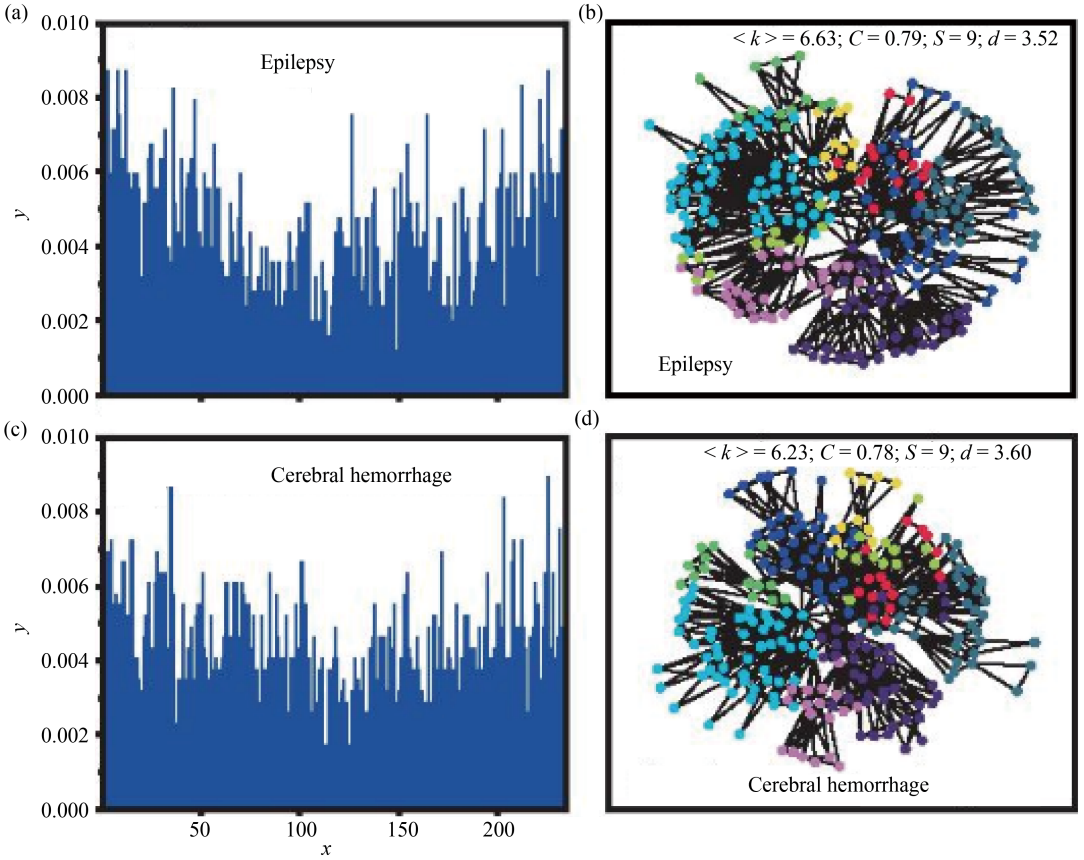

Figure 5. Time series and network structures of two neurological disorders. (a) and (c) are the time series of epilepsy and cerebral haemorrhage, respectively. (b) and (d) are their corresponding network structures, respectively. Different colors represent different communities

Finally, we turn to the analysis of neurological diseases, represented by epilepsy and cerebral hemorrhage, whose network architectures are displayed in Figure 5. Both networks consistently exhibit high clustering coefficients-yielding values of $C = 0.79$ for epilepsy and $C = 0.78$ for cerebral hemorrhage-accompanied by short average shortest path

lengths, with $< d >= 3.52$ and $< d >= 3.60$, respectively. These features reaffirm the presence of a pronounced small-world topology across disease categories. Notably, the average degrees $< k >$ of epilepsy and cerebral hemorrhage in the neurological disease network were 6.63 and 6.23 respectively - lower than those in the respiratory disease network. This indicates a comparatively sparser yet efficiently organized connectivity pattern. Additionally, diverse community structures S are observable within these networks.

Through a comparison of network structures across the four disease categories, we observed that all constructed networks exhibit high clustering coefficients C and short average path lengths $< d >$. To enhance the reliability of our conclusions, the analysis was expanded from two to four diseases per category, resulting in a total of 16 diseases. The structural statistical parameter in Figure 6, including the clustering coefficient C, average shortest path length $< d >$, average degree $< k >$, and number of community structures S for each disease. Each category is represented by a distinct color, with four diseases included per group.

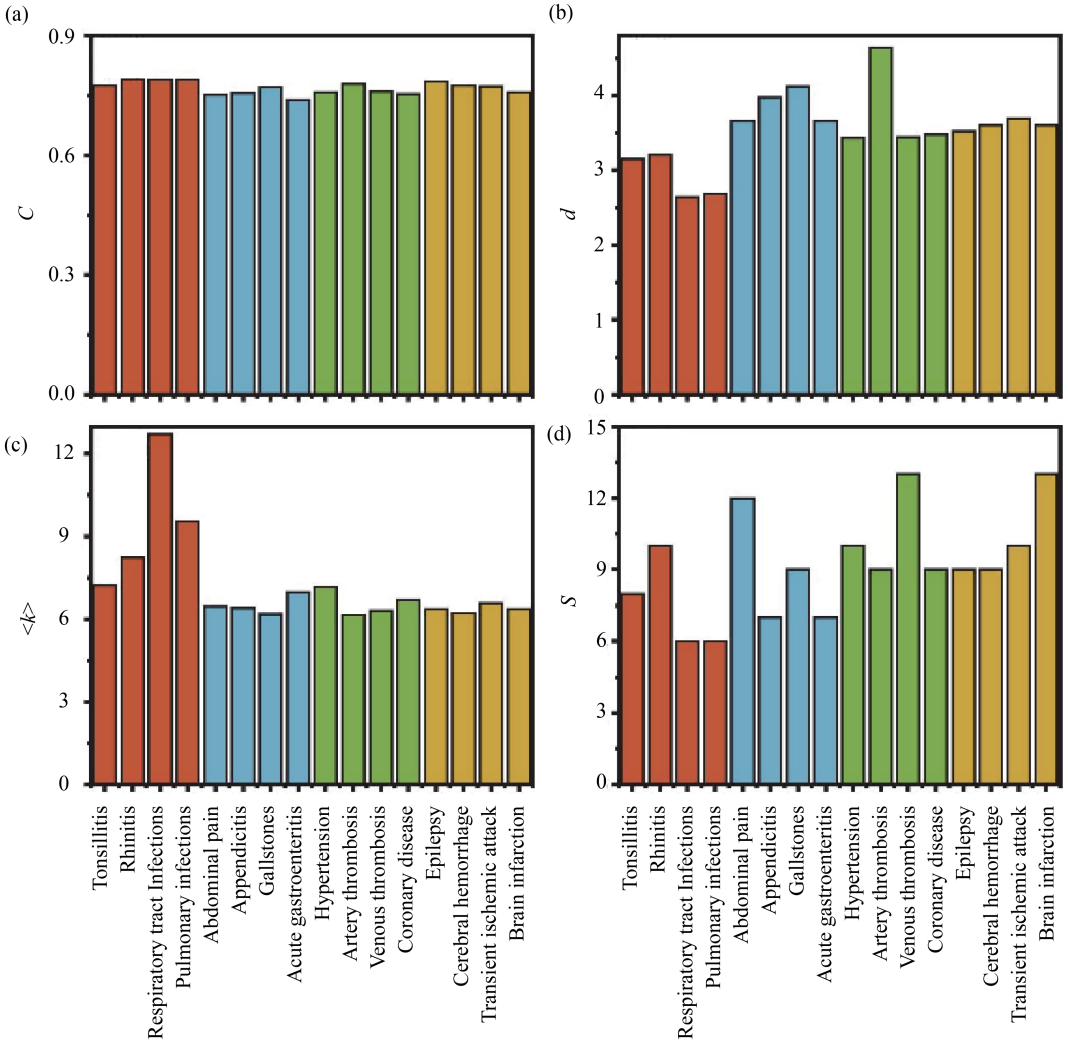

Figure 6. The histogram of different structural statistical parameters of the 16 disease networks. (a)-(d) are the cluster coefficients C, the average shortest path $< d >$, the average degree $< k >$ and number of communities S, respectively. Different colored bars represent various categories of diseases, arranged from left to right as respiratory, digestive, circulatory, and neurological

As shown in Figure 6a, the clustering coefficients C for nearly all networks are notably high, with most values concentrated around 0.8. Figure 6b reveals that the average shortest path lengths $< d >$ for all 16 diseases remain

consistently low. Notably, respiratory diseases display the smallest $< d >$ values among all categories, suggesting superior information propagation efficiency. The combination of high cluster coefficients C and small average shortest paths $< d >$ imply that there is a strong small-world effect within this network [37], indicating that the small-world effect of the network composed of respiratory diseases is stronger than other categories of diseases. Furthermore, as illustrated in Figure 6c, respiratory diseases also show a higher average degree $< k >$ compared to the other three categories, reflecting denser connectivity within these networks. Finally, Figure 6d indicates that respiratory disease networks contain significantly fewer community structures S than those of digestive, circulatory, or neurological diseases. This structural coherence further supports the notion of tighter integration and more homogeneous connectivity patterns in respiratory disease networks, consistent with their high transmissibility and rapid spread dynamics.

From the above analysis, we know that the respiratory disease network has a smaller average shortest path d and a larger average degree $< k >$. This divergence suggests that respiratory diseases are different with other three categories of diseases. Furthermore, we know that denser connectivity within a network, indicated by a larger average degree $< k >$, correlates with a smaller average shortest path $< d >$. This implies that shorter distances and smaller number of community structures S between nodes within the network facilitate easier transmission of information, including the transmission of diseases.

3.2 *Analysis from network Laplacian matrix eigenvalues*

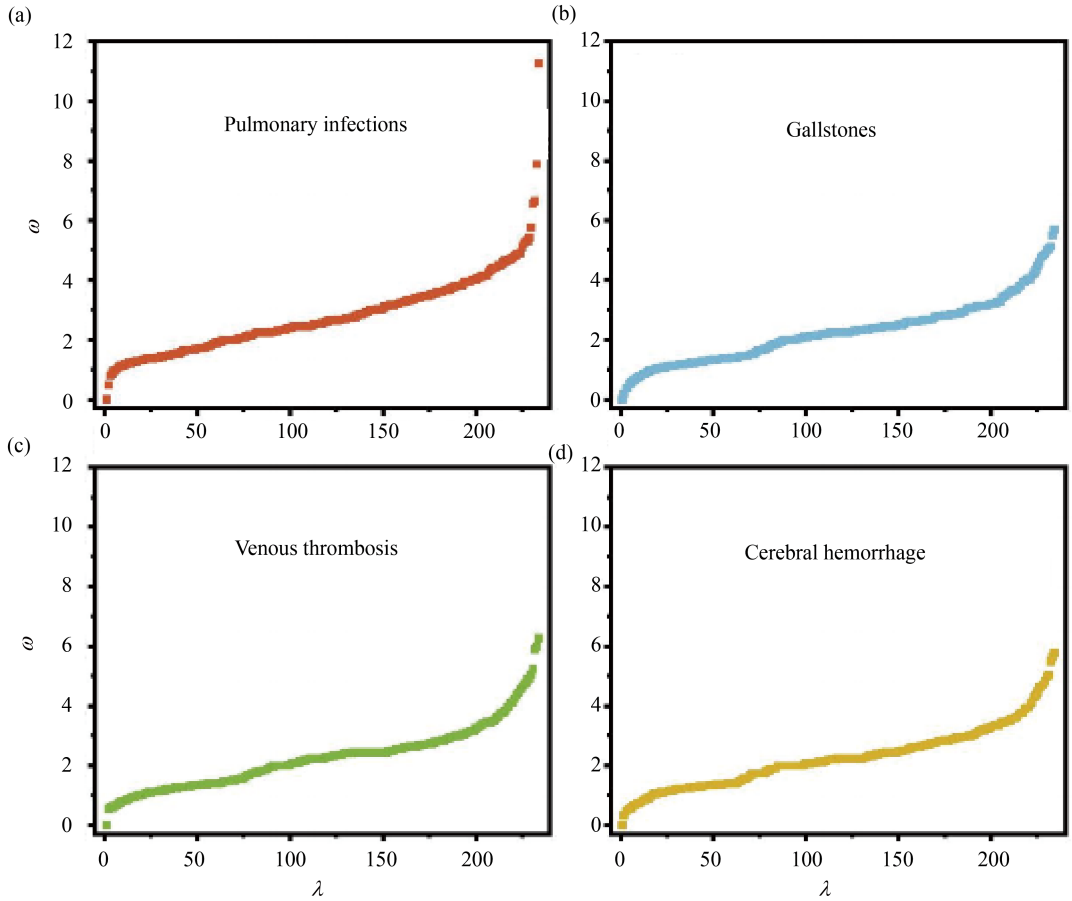

Figure 7. The influence of different disease networks on eigenvalues. (a-d) The eigenfrequency ω versus its eigenmode index λ for pulmonary infection (respiratory system), gallstones (digestive system), venous thrombosis (circulatory system) and cerebral hemorrhage (nervous system and circulatory system), respectively

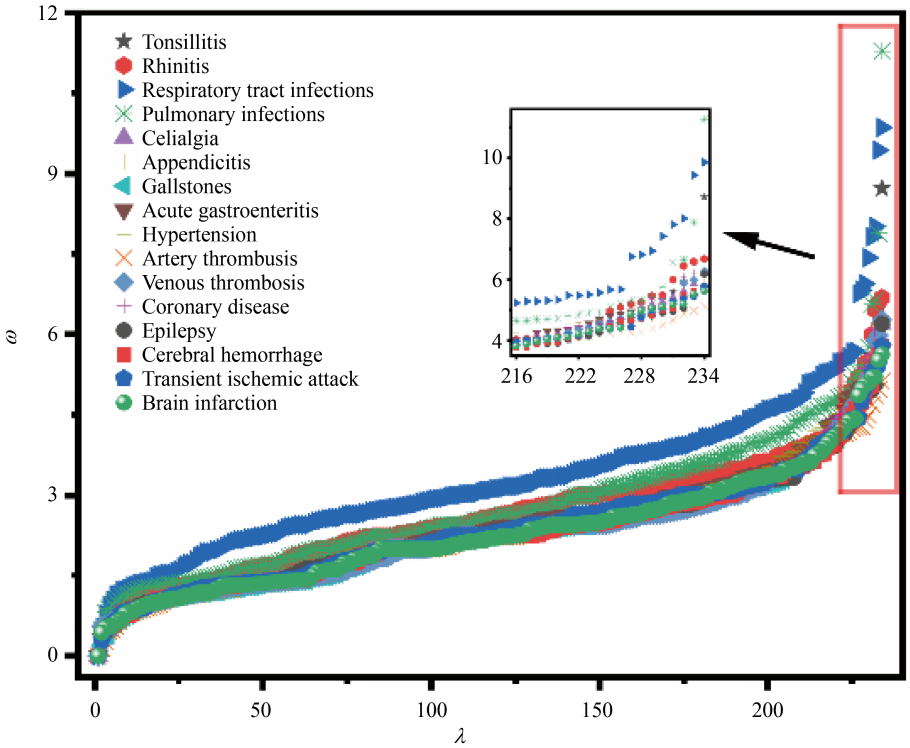

Figure 8. The eigenfrequency ω versus its eigenmode index λ for 16 disease networks

The eigenspectrum of the Laplace matrix plays a pivotal role in comprehending and analyzing the structure, properties, and behavior of graphs [38–40]. Notably, the largest eigenvalue holds significance in graph theory and network analysis. Generally, the largest eigenvalue of the Laplace matrix corresponds to some global property of the graph and also reflects aspects such as system synchronization [41], dynamic behavior [42]. Therefore, we can delve into its properties by calculating the maximum eigenvalue of the network. First, we calculate the eigenvalues of the network by arbitrarily picking one disease for each category of disease. Given the adjacency and degree matrices of a network, its Laplace matrix is

$$L = D - A, \tag{2}$$

where A represents the adjacency matrix. If there is a connecting edge between node i and node j, then $A(i,\ j) = 1$, otherwise $A(i,\ j) = 0$. The matrix D is a diagonal matrix denoted as $D_{i,\ j} = \delta_{i,\ j}k_i$. With the Laplace matrix, we can derive the eigenvalues of the network [38].

To further investigate the spectral characteristics of disease networks, we selected one representative from each category: pulmonary infections (respiratory system), gallstones (digestive system), venous thrombosis (circulatory system), and cerebral hemorrhage (neurological system). The eigenvalue spectra of these networks are presented in Figure 7. In all cases, the eigenvalues are ordered increasingly from zero, consistent with the properties of Laplacian matrices. A striking observation is that the maximum eigenvalue $\omega_{\max}$ corresponding to pulmonary infections significantly exceeds those of the other three diseases, exhibiting a twofold difference. This pronounced discrepancy highlights a strong association between the maximum eigenvalue of the network Laplacian and the infectious potential of the disease.

We further extended this spectral analysis to all 16 diseases, with the full eigenvalue distributions illustrated in Figure 8. The results show that pulmonary infections exhibits the largest $\omega_{\max}$ among all networks, followed closely by respiratory

tract infections, Tonsillitis, and Rhinitis. Notably, all four diseases with the highest maximum eigenvalues belong to the respiratory category, reinforcing the link between elevated $\omega_{\max}$ and high infectivity. This pattern suggests that respiratory diseases not only display distinctive topological properties but also singular spectral features associated with rapid transmission and population-level susceptibility. Consequently, these findings underscore the need for heightened preventive measures against respiratory infections.

Based on these consistent results, we propose the maximum eigenvalue max of the network Laplacian as a quantitative indicator of disease infectivity. Its robustness across diseases within the same category and discriminative power across categories make it a promising tool for evaluating epidemic risk from complex network perspectives.

4. Conclusion and discussion

4.1 *Conclusion*

In this paper, our focus lies on the time series and network structure of four disease categories: respiratory system, digestive system, circulatory system, and nervous system. Previous approaches have largely emphasized sequence visualization while ignoring the network topology [43, 44]. By transforming time series into complex networks using visibility graph methods, we analyze key topological properties including the average degree $< k >$, the average shortest path $< d >$, the clustering coefficient C, and the number of community structures S. Our findings reveal that all constructed networks exhibit higher clustering coefficients, while the average shortest paths for respiratory disease networks are notably lower than those of the other three categories, indicating a stronger small-world effect. The observed higher clustering coefficient in respiratory disease networks reflects their tendency to form tightly connected clusters, which correlates with the rapid transmission patterns typical of respiratory infections. The shorter average path length indicates efficient propagation pathways through the network, explaining why respiratory outbreaks can spread more quickly through populations compared to other diseases. In addition, we observe that the average degree $< k >$ of respiratory disease networks is generally higher than in the other categories. Additionally, by calculating the spectral properties of these networks, we find that larger maximum Laplacian eigenvalues correlate with greater epidemic risk. We propose using the maximum eigenvalue, denoted $\omega_{\max}$, as a quantitative indicator of disease infectivity. These network characteristics offer actionable insights for emergency departments, enabling more effective mitigation of transmission risks. Therefore, this method can be strategically applied in disease prevention to better anticipate and respond to outbreaks.

4.2 *Discussion*

The spectrum of the Laplacian matrix, particularly its maximum eigenvalue ($\omega_{\max}$), is a cornerstone in understanding the synchronization dynamics and stability of complex systems. A larger $\omega_{\max}$ indicates a higher synchronizability of the network. Physically, this translates to a population that is more susceptible to coordinated, large-scale outbreaks. The disease dynamics can synchronize more easily across different time points and population subgroups, leading to the characteristic explosive growth seen in respiratory epidemics. Conversely, a smaller $\omega_{\max}$ for other diseases suggests a more disordered, less synchronized pattern of incidence, which is consistent with their non-communicable or slower-spreading nature.

Our findings suggest concrete applications for public health practice. For example, real-time monitoring of $\omega_{\max}$ for specific disease time series could serve as a structural early-warning system, providing earlier indicators of impending epidemics than traditional surveillance metrics. Therefore, this method can be strategically applied in disease prevention to better anticipate and respond to outbreaks.

Despite the promising results, this study has limitations that also point to valuable directions for future research. The use of data from a single center may affect the generalizability of our findings, requiring validation with multi-center data. Furthermore, the HVG method focuses on intrinsic temporal patterns and does not account for external variables (e.g., seasonality, policy changes, public health interventions). Future work could integrate these exogenous factors into a multilayer network framework to disentangle their influence on the observed network topology and disease dynamics.

Additionally, the correlational nature of our analysis necessitates further work to establish causality. Finally, exploring alternative network mapping techniques, such as the Weighted Visibility Graph or Recurrence Networks, could provide a more nuanced representation of the time series data and potentially yield even more discriminative structural features for epidemic surveillance.

Funding

This work was supported by the Key Research and Development Programme of Shaanxi Province (2023-YBGY-147, 2024SF-YBXM-666); the Air Force Medical University Interdisciplinary Integration Special Project (2024JC059); the Military Nursing Innovation and Cultivation Special Program (2023HL040, 2023HL008); the National Natural Science Foundation of China (12005166); and the China Postdoctoral Science Foundation (2022M720036, 2023T160110).

Conflict of interest

The authors declare no competing financial interest.

References

[1] Wu H, Song C, Ge Y, Ge T. Link prediction on complex networks: an experimental survey. *Data Science and Engineering*. 2022; 7(3): 253-278.

[2] Sedghi L, DiMassa V, Harrington A, Lynch SV, Kapila YL. The oral microbiome: role of key organisms and complex networks in oral health and disease. *Periodontology 2000*. 2021; 87(1): 107-131.

[3] Van Mil HG, Foegeding E, Windhab EJ, Perrot N, Van der Linden E. A complex system approach to address world challenges in food and agriculture. *Trends in Food Science & Technology*. 2014; 40(1): 20-32.

[4] Xiong K, Yan Z, Xie Y, Liu Z. Regulating heat conduction of complex networks by distributed nodes masses. *Scientific Reports*. 2021; 11(1): 5501.

[5] Albert R, Barabási AL. Statistical mechanics of complex networks. *Reviews of Modern Physics*. 2002; 74(1): 47.

[6] Barabási AL, Gulbahce N, Loscalzo J. Network medicine: a network-based approach to human disease. *Nature Reviews Genetics*. 2011; 12(1): 56-68.

[7] Jacunski A, Tatonetti N. Connecting the dots: applications of network medicine in pharmacology and disease. *Clinical Pharmacology & Therapeutics*. 2013; 94(6): 659-669.

[8] Wu T, Huo S, Alfaro-Bittner K, Boccaletti S, Liu Z. Double explosive transition in the synchronization of multilayer networks. *Physical Review Research*. 2022; 4(3): 033009.

[9] Zhou JF, Jiang EH, Xu BL, Xu K, Zhou C, Yuan WJ. Synaptic changes modulate spontaneous transitions between tonic and bursting neural activities in coupled Hindmarsh-Rose neurons. *Physical Review E*. 2021; 104(5): 054407.

[10] Arenas A, Fernandez A, Gomez S. Analysis of the structure of complex networks at different resolution levels. *New Journal of Physics*. 2008; 10(5): 053039.

[11] Christakis NA, Fowler JH. Social contagion theory: examining dynamic social networks and human behavior. *Statistics in Medicine*. 2013; 32(4): 556-577.

[12] Alm E, Arkin AP. Biological networks. *Current Opinion in Structural Biology*. 2003; 13(2): 193-202.

[13] Oyewole AT, Adeoye OB, Addy WA, Okoye CC, Ofodile OC, Ugochukwu CE. Predicting stock market movements using neural networks: a review and application study. *Computer Science & IT Research Journal*. 2024; 5(3): 651-670.

[14] Zhen Z, Bo Ma XW, Zhao H, Zhang Y. Propagation network of tailings dam failure risk and the identification of key hazards. *Scientific Reports*. 2022; 12: 5580.

[15] Stegehuis C, Van der Hofstad R, Van Leeuwaarden JS. Epidemic spreading on complex networks with community structures. *Scientific Reports*. 2016; 6(1): 29748.

[16] Zhou Y, Wang Y, Li C, Ding L, Mei Y. Coupled risk analysis of hospital infection: a multimethod-fusion model combining association rules with complex networks. *Computers & Industrial Engineering*. 2023; 186: 109720.
[17] Gawęda Ł, Pionke R, Hartmann J, Nelson B, Cechnicki A, Frydecka D. Toward a complex network of risks for psychosis: combining trauma, cognitive biases, depression, and psychotic-like experiences on a large sample of young adults. *Schizophrenia Bulletin*. 2021; 47(2): 395-404.
[18] Ranjbari S, Khatibi T, Vosough Dizaji A, Sajadi H, Totonchi M, Ghaffari F. CNFE-SE: a novel approach combining complex network-based feature engineering and stacked ensemble to predict the success of intrauterine insemination and ranking the features. *BMC Medical Informatics and Decision Making*. 2021; 21: 1-29.
[19] Hammoud Z, Kramer F. Multilayer networks: aspects, implementations, and application in biomedicine. *Big Data Analytics*. 2020; 5(1): 2.
[20] Kinsley AC, Rossi G, Silk MJ, VanderWaal K. Multilayer and multiplex networks: an introduction to their use in veterinary epidemiology. *Frontiers in Veterinary Science*. 2020; 7: 596.
[21] Taylor GJ. Recent developments in alexithymia theory and research. *The Canadian Journal of Psychiatry*. 2000; 45(2): 134-142.
[22] English S, Barreaux AM, Bonsall MB, Hargrove JW, Keeling MJ, Rock KS, et al. Incorporating vector ecology and life history into disease transmission models: insights from tsetse (*Glossina* spp.). In: *Population Biology of Vector-Borne Diseases*. Oxford: Oxford University Press; 2021. p.175-188.
[23] Busenberg S, Van den Driessche P. Analysis of a disease transmission model in a population with varying size. *Journal of Mathematical Biology*. 1990; 28(3): 257-270.
[24] Morid MA, Sheng ORL, Dunbar J. Time series prediction using deep learning methods in healthcare. *ACM Transactions on Management Information Systems*. 2023; 14(1): 1-29.
[25] Aydin S. Time series analysis and some applications in medical research. *Journal of Mathematics and Statistics Studies*. 2022; 3(2): 31-36.
[26] Hadwan M, Al-Maqaleh BM, Al-Badani FN, Khan RU, Al-Hagery MA. A hybrid neural network and Box-Jenkins models for time series forecasting. *Computers, Materials & Continua*. 2021; 7(3): 4829-4845.
[27] Vulliard L, Menche J. Complex networks in health and disease. In: *Systems Medicine*. New York: Humana Press; 2021. p.26-33.
[28] Milad Y, Moslem Y, Masood F, Fogliatto FS. Patient visit forecasting in an emergency department using a deep neural network approach. *Kybernetes*. 2020; 49(9): 2335-2348.
[29] Hackl J, Scholtes I, Petrović LV, Perri V, Verginer L, Gote C. Analysis and visualisation of time series data on networks with Pathpy. In: *Companion Proceedings of the Web Conference 2021*. Ljubljana, Slovenia: Association for Computing Machinery; 2021. p.530.
[30] Leporowski B, Iosifidis A. Visualising deep network time-series representations. *Neural Computing and Applications*. 2021; 33(23): 16489-16498.
[31] Luque B, Lacasa L, Ballesteros F, Luque J. Horizontal visibility graphs: exact results for random time series. *Physical Review E*. 2009; 80: 046103.
[32] Lacasa L, Luque B, Ballesteros F, Luque J, Nuño JC. From time series to complex networks: the visibility graph. *Proceedings of the National Academy of Sciences*. 2008; 105(13): 4972-4975.
[33] Xie WJ, Zhou WX. Horizontal visibility graphs transformed from fractional Brownian motions: topological properties versus the Hurst index. *Physica A: Statistical Mechanics and Its Applications*. 2011; 390(20): 3592-3601.
[34] Chomiak T, Hu B. Time-series forecasting through recurrent topology. *Communications Engineering*. 2024; 3: 9.
[35] Albert R, Barabási AL. Statistical mechanics of complex networks. *Reviews of Modern Physics*. 2002; 74(1): 47.
[36] Clauset A. Finding local community structure in networks. *Physical Review E*. 2005; 72(2): 026132.
[37] Watts DJ, Strogatz SH. Collective dynamics of 'small-world' networks. *Nature*. 1998; 393(6684): 409-410.
[38] Peixoto TP. Eigenvalue spectra of modular networks. *Physical Review Letters*. 2013; 111(9): 098701.
[39] Mitrović M, Tadić B. Spectral and dynamical properties in classes of sparse networks with mesoscopic inhomogeneities. *Physical Review E*. 2009; 80(2): 026123.
[40] McGraw PN, Menzinger M. Laplacian spectra as a diagnostic tool for network structure and dynamics. *Physical Review E*. 2008; 77(3): 031102.
[41] Barahona M, Pecora LM. Synchronization in small-world systems. *Physical Review Letters*. 2002; 89(5): 054101.
[42] Milanese A, Sun J, Nishikawa T. Approximating spectral impact of structural perturbations in large networks. *Physical Review E*. 2010; 81(4): 046112.

[43] Lacasa L, Luque B, Ballesteros F, Luque J, Nuño JC. From time series to complex networks: the visibility graph. *Proceedings of the National Academy of Sciences*. 2008; 105(13): 4972-4975.
[44] Gao Z, Jin N. Complex network from time series based on phase space reconstruction. *Chaos*. 2009; 19(3): 033137.